Title

Mg^{2+}-free ATP Regulates Native Cytoplasmic Dynein's Processivity

Author names and affiliations

VA Behrens[1,*], WJ Walter[1,3,*], C Peters[1,2], T Wang[1], B Brenner[1], MA Geeves[4], T Scholz[1,5, #], W Steffen[1,5, #]

[*] These co-first authors contributed equally to this work.

[#] These co-last authors contributed equally to this work.

[1]Molecular and Cellular Physiology, Hannover Medical School, Carl-Neuberg-Strasse 1, 30625 Hannover, Germany

[2]present address: Center for Integrated Protein Science and Department Chemie, Technische Universität München, 85748 Garching, Germany

[3]present address: Molecular Plant Physiology, Institute for Plant Science and Microbiology, University of Hamburg, 22609 Hamburg, Germany

[4]School of Biosciences, University of Kent, Canterbury, Kent, UK

[5]To whom correspondence should be addressed: Tim Scholz, Tel: +49-511-5322737; Fax: +49-511-5324296; E-mail: scholz.tim@mh-hannover.de; or Walter Steffen, Tel: +49-511-5322754; Fax: +49-511-5324296; E-mail: Steffen.Walter@MH-Hannover.de, Molecular and Cellular Physiology, Hannover Medical School, Carl-Neuberg-Strasse 1, 30625 Hannover, Germany.

Abstract

Cytoplasmic dynein, a microtubule-based motor protein is responsible for many cellular functions ranging from cargo transport to cell division. The various functions are carried out by a single isoform of cytoplasmic dynein, thus requiring different forms of motor regulation. A possible pathway to regulate motor function was revealed in optical trap experiments. Switching motor function from single steps to processive runs could be achieved by changing Mg^{2+} and ATP concentrations. Here we confirm by single molecule TIRF microscopy that a native cytoplasmic dynein dimer is able to switch to processive runs of more than 680 consecutive steps or 5.5 micrometres. We also identified the ratio of Mg^{2+}-free ATP to Mg.ATP as the regulating factor and propose a model for dynein processive stepping.

Keywords

cytoplasmic dynein, processivity, regulation, Mg^{2+}-free ATP, single molecule experiment

Abbreviations

Microtubule – MT
Microtubule-binding domain – MTBD
Single molecule motility assay – SMM assay
Total internal reflection fluorescence microscope – TIRF microscope

Conflict of interest

All authors disclose any actual or potential conflict of interest including any financial, personal or other relationships with other people or organizations within three years of beginning the submitted work that could inappropriately influence, or be perceived to influence, their work.

Author Contributions

WS and VB conceived the study, which was supervised by WS, MG, TS and BB. VB, WS, MG, and TS designed experiments. VB, TS, WJW, TW, and CP performed experiments. Proteins were purified by VB and TW. VB, TS, WS, WJW, TW, and CP analysed data. VB, TS, and WJW wrote the manuscript with revisions from WS and MG.

Funding source

DFG provided financial support to WS (STE 1697/1-2).

Introduction

Cytoplasmic dynein is an ATP-driven, microtubule-based molecular motor with many different functions ranging from intracellular vesicle transport to spindle formation [1]. To move a cargo along a microtubule as a single motor molecule, dynein needs to undertake consecutive steps without detaching from its track, i.e., it moves processively. *In vivo*, long-haul single motor movement is supported by several accessory proteins. Dynein's best-studied interaction partner is dynactin [2] which has been shown to enhance processivity by stabilizing the microtubule-motor interaction [3] and by dimerization of dynein heavy chain dimers [4,5]. Moreover, effectors interacting with dynein's Light Intermediate Chain 1 (LIC1) can enhance motility [6]. Yet, several *in vitro* studies showed processive movement of single dynein motors even in absence of accessory proteins suggesting intrinsic processive properties of dynein.

The dynein motor complex consists of two identical heavy chains and several light and intermediate chains. Each heavy chain has a mass of ~520 kDa and contains the microtubule-binding domain (MTBD), a catalytic ring structure, and a tail region used for dimerization. The tail region serves also as a binding site for light and intermediate chains and as an interaction site for accessory proteins and protein complexes needed for cargo binding [7,8].

Crystallisation of the motor domain, a C-terminal 380 kDa fragment of the heavy chain, has revealed a number of subdomains [9-11], most importantly the catalytic domain which is composed of a ring structure of six AAA (ATPase associated with various cellular activities) domains [12]. In contrast to other AAA-domain proteins, only AAA1-4 possess conserved P-loops and only AAA1, 3, and 4 are enzymatically active, while AAA5-6 appear to have rather structural functions [9,13] (review in [14]). AAA1 was found to be essential for dynein's chemomechanical ATPase cross-bridge cycle [15]. AAA2-4 also bind and hydrolyse Mg.ATP but at lower rates than AAA1 [16,17]. The MTBD is located at the end of a stalk-like structure [18,19]. The nucleotide states of AAA2-4 appear to modulate a possible communication pathway between AAA1 and the remote MTBD and thereby the dynein-microtubule interaction [16]. The stalk is formed by a pair of antiparallel alpha-helices which emerge from the ring-like motor domain between AAA4 and AAA5. A shift in the alignment of these alpha-helices can modulate the microtubule affinity of the globular MTBD [20-22]. A linker domain, which connects the motor domain with the dimerization domain of the tail region, emerges from the N-terminus of the sub-domain AAA1. During the ATPase cross-bridge cycle this linker can undergo conformational changes from straight to bend conformation and vice versa. It had been proposed that bending of the linker domain may act like a lever between the catalytic ring domain and the tail. The conformational state of the linker appears to depend on the nucleotide state of AAA1 [23], but may also be affected by the other AAA domains [3]. For processive movement, the linker domain has to alternate between straight and bent conformations. Thus, factors that interfere with such alternations might result in slower and/or terminated movements.

Cytoplasmic dynein is a microtubule-activated Mg-ATPase. While Mg^{2+}-free ATP is not hydrolysable by dynein [24] force generation is coupled to binding and hydrolysis of Mg.ATP by

AAA1 [16]. In previously reported optical trap experiments, we could demonstrate that cytoplasmic dynein can switch from single binding events to processive movement by modulating the concentration of free Mg^{2+} at a constant low ATP concentration of 1 µM [25]. Decreasing the concentration of Mg^{2+} from 1 mM to 0.1 mM, while keeping ATP at 1 µM, enabled dynein to perform multiple consecutive steps. Processive movement was also observed when the concentration of ATP was increased from 1 µM to 100 µM at a constant Mg^{2+} concentration of 1 mM. Mg^{2+} ions and ATP form stable Mg.ATP complexes and the degree of complex formation depends on the ratio of Mg^{2+} to ATP. Lowering the Mg^{2+} concentration will not only affect the Mg.ATP complex concentration but will also increase the concentration of Mg^{2+}-free ATP. Thus, it remained unclear, if the switch in dynein's processivity was caused by free Mg^{2+}, by Mg^{2+}-free ATP, or by the ratio of Mg^{2+}-free ATP to Mg.ATP.

To characterize the effects of Mg^{2+} and ATP nucleotides on the regulation of dynein's motor function we made use of *in vitro* microtubule gliding assays, TIRF microscopy single molecule motility assays, as well as ATPase and transient kinetic measurements in a stopped-flow set up. We could verify that dynein's processivity can be regulated independently of accessory proteins and protein complexes such as BICD2 or dynactin [25] and identified the ratio of Mg^{2+}-free ATP to Mg.ATP as the regulating factor. Based on our findings we propose a model for dynein processive stepping dependent upon the nucleotide state of dynein's AAA4 domain. The existence of more than one independent method to trigger dynein's processivity might help to explain, how dynein may master such a wide variety of functions in cells.

Methods

Protein purification, labelling, and microtubule polymerisation

Cytoplasmic dynein was isolated and purified from pig brain tissue as described by Bingham *et* al. and Toba *et al.* [26,27] with a minor modification [28]: a filtration step (10 µm filter) was added prior SP-Sepharose ion exchange chromatography. Purification of tubulin from pig brain tissue and labelling with Cy5- and rhodamine fluorophores was basically performed as described by others [29,30]. The dynein-intermediate chain antibody m74-2 [31] was labelled with rhodamine using the Pierce™ NHS-Rhodamine Antibody Labeling Kit (Thermo Fisher Scientific, 53031).

Optical trap experiments

Two bead optical trap experiments were carried out as described previously [32]. A polyclonal antibody specific for the minus-end of microtubules was used to attach microtubule seeds to protein A/G coated 1 µm latex beads [25]. Polyclonal antibodies specific for the minus-end of microtubules were raised in rabbits against two synthetic peptides from bovine α-tubulin and purified using a protein G affinity column. As highlighted in yellow and magenta (**Fig. S3**, based on PDB structure 1JFF) the following peptides of α-tubulin have been used for antibody production: peptide 1: aa31-

40 (QPDGQ MPSDK) and peptide 2: aa242-255 (LRFDG ALNVD LTEF). The microtubule seeds were extended using a mixture of rhodamine and biotin-labelled tubulin. A bead with a single microtubule attached was captured in one of the optical traps and a second, neutravidin-coated bead was attached laterally near the plus-end of this microtubule using the second trap. The two bead-microtubule construct was stretched taught and presented above a dynein molecule immobilized on top of a fixed glass bead. Two experimental conditions are shown: (i) processive conditions with 35 mM K-Pipes, pH 7.4, 1 mM EGTA, 1 µM ATP, 0.1 mM $MgCl_2$ (**Fig. 1A**) and (ii) non-processive conditions with 35 mM K-Pipes, pH 7.4, 1 mM EGTA, 1 µM ATP, 1 mM $MgCl_2$ (**Fig. 1B**).

Gliding assay

0.2% nitrocellulose coated flow chambers were incubated with 0.2 mg/ml dynein in BRB35 (35 mM K-PIPES, 1 mM EGTA, 1 mM $MgCl_2$, 1 mM DTT, pH 7.4) for 2 min. After blocking with 10 mg/ml bovine serum albumin (BSA) in BRB35 for 5 min the dynein-coated chamber was incubated with 10 µg/ml rhodamine-labelled microtubules in the absence of ATP. After 10 min incubation, most non-attached microtubules were washed out. Microtubule gliding velocities at increasing Mg.ATP concentrations were characterized at room temperature in buffer BRB containing 100 mM K-PIPES (**Fig. 2A**). Gliding assays with increasing concentrations of magnesium were carried out in BRB35 containing constant 0.1 mM ATP and varying concentrations of $MgCl_2$ as indicated (**Fig. 2B**). The final ionic strength was adjusted to 115 mM using KCl. Experiments shown in Figure **2C** were performed either with 0.55 mM $MgCl_2$ plus 0.9 mM ATP or with 6 mM $MgCl_2$ plus 0.5 mM ATP in 10 mM K-PIPES containing 0.5 mM EGTA. The ionic strength of both solutions was adjusted to 30 mM using KCl. The final concentrations of Mg^{2+}, Mg.ATP and Mg^{2+}-free ATP were calculated with the Maxchelator program (http://maxchelator.stanford.edu/CaMgATPEGTA-TS.htm; [33]). To keep ATP levels constant an ATP regeneration system containing 2 mM creatine phosphate and 10 U/ml creatine kinase was added. Gliding velocities were analysed with ImageJ (W.S. Rasband, National Institutes of Health, Bethesda, MD) using the plug-in MtrackJ [34].

Single molecule motility assay by TIRF microscopy

Single molecule motility (SMM) assays were carried out at 23°C in a custom-made TIRF microscope with single-fluorophore sensitivity [35] using paclitaxel-stabilized Cy5-labelled microtubules and native pig brain cytoplasmic dynein. The cytoplasmic dynein was tagged with a rhodamine-labelled intermediate-chain specific antibody [31]. To form antibody-dynein complexes 200 nM cytoplasmic dynein and 150 nM fluorescently labelled antibodies were pre-incubated in BRB35 buffer on ice for 20 min. For TIRF microscopy antibody-labelled dynein was diluted to a final concentration of 0.3 nM. Prior to injection of dynein, fluorescently labelled microtubules were immobilized by a β-tubulin antibody (SAP.4G5, Santa Cruz) to the dichlorodimethylsilane functionalized bottom of the assay chamber as described previously [36]. Two experimental conditions were used: 12 mM K-PIPES with 0.5 mM EGTA, 6 mM $MgCl_2$, and 0.5 mM ATP (resulting in 0.5 mM Mg.ATP and < 10 µM Mg^{2+}-free ATP) and 28.6 mM K-PIPES with 0.5 mM EGTA, 0.55 mM $MgCl_2$, and 0.9 mM ATP (resulting in 0.5 mM Mg.ATP and 400 µM Mg^{2+}-free ATP), both conditions with an equal ionic strength of 30 mM. To minimize photo damage or bleaching of fluorophores the buffers were supplemented with an oxygen scavenger system (10 mg/ml glucose, 50 U/ml glucose oxidase, 7600 U/ml catalase, and 10mMDTT). Additionally, 50 µs laser pulses interrupted by 50 µs pauses were used to excite the fluorescently labelled samples [36]. Video images were recorded at 5Hz for 60 seconds using a back-illuminated EMCCD camera (Andor iXon DV887, Andor Technology, Belfast, Ireland) and analysed as described previously [35] using the computer program ImageJ, the plug-in Multiple Kymograph (J. Rietdorf and A. Seitz, EMBL, Heidelberg, Germany) and the macro ListSelectionCoordinates. To distinguish processive runs from unproductive binding events only trajectories of at least 0.5 µm (approx. three pixels of 156 nm each) were analysed.

ATPase assay

ATPase assays [37] were performed with the EnzChek Phosphate Assay Kit (Thermo Fisher, E-6646). Buffer conditions were the same as in the gliding assay (**Fig. 2C**). Protein concentrations were 0.07 mg/ml dynein and 0.02, 0.1, 0.5, or 1 mg/ml microtubules, respectively.

Transient kinetic stopped-flow measurements

Common stopped-flow experiments require a large amount of protein, typically approx. 1 ml of each of the two solutions to be mixed [38] because of the large volumes required to fill the apparatus. To conserve material we employed a newly developed micro-volume manifold system (J. Walklate, 2016, PhD Thesis, University of Kent) attached to a HITECH stopped flow system. The manifold allowed a 100 µl slug of the dynein/microtubule solution to be loaded into the flow circuit just before the mixing chamber. Standard reaction buffer in the syringe was then used to drive this solution through the mixing chamber where 10 µl of the dynein/microtubule solution was mixed with an equal volume of ATP containing solution in each shot. Using a 5 µl observation chamber allowed 8 reproducible shots of the reaction to be collected consecutively with a 1 ms dead time. Transient changes in 90° light scattering were recorded using a 365 nm LED excitation light source. Dynein-microtubule complexes were pre-formed by incubating 1 µM paclitaxel-stabilized polymerised tubulin (microtubules) and 140 nM dynein for 20 min at 25°C. The complex suspension was diluted 1:5 before rapid mixing with an ATP containing solution in the stopped-flow setup. Protein concentrations after mixing were 100 nM polymerised tubulin stabilized with 5 µM paclitaxel and 14 nM dynein. Mg.ATP induced dissociation of the complex was observed by a decrease in light scattering. Experimental conditions were set to 50 µM Mg.ATP either using total concentrations of (i) 53 µM Mg^{2+} and 450 µM ATP (high concentration of Mg^{2+}-free ATP) or of (ii) 2 mM Mg^{2+} and 50 µM ATP (low concentration of Mg^{2+}-free ATP), all in buffer BRB10 and at 16 mM ionic strength (adjusted with KCl), 5 µM paclitaxel and 5 mM DTT.

Results

Lowering the concentration of free Mg^{2+} increases dynein‘s processivity and velocity in optical tweezer experiments

Using an optical trap we observed that even in the absence of accessory proteins such as dynactin cytoplasmic dynein could be turned from a non-processive to a processive motor by reducing the concentration of free Mg^{2+} [25]. In the presence of 1 µM ATP and 1 mM $MgCl_2$ dynein molecules showed a non-processive binding/release behaviour with an apparent working stroke of approximately 8 nm towards the minus-end of microtubules (-8.7 nm ± 0.25, fit error, n=900 events from 14 dynein molecules, **Fig, 1B**). A reduction of $MgCl_2$ to 0.1 mM in addition to constant 1 µM ATP led to repetitive processive runs with consecutive steps of approximately -8 nm (n>600 events from 6 dynein molecules with multiple processive runs of up to 10 steps per run, **Fig. 1A**). We also noticed that the life time of consecutive steps in these experiments increased with increasing load (**Fig. 1A**). A closer examination revealed that the life time of the initial steps of processive runs was significantly shorter (~25 ms/step for the initial three steps) than single microtubule binding events (107 ms ± 3.3, fit error, n=900 events from 14 dynein molecules) under non-processive conditions (**Fig. 1**). Lowering the concentration of free Mg^{2+} appears to lead to a combined increase of dynein’s processivity and velocity. This effect could be caused by either the decreasing Mg^{2+} concentration or the resulting increasing ratio of Mg^{2+}-free ATP to Mg.ATP (**Tab. 1**). As previous studies have shown that different nucleotide states of the AAA domains modulate dynein‘s overall ATPase activity and motility [16], we hypothesized that the ratio of Mg^{2+}-free ATP to Mg.ATP and not free Mg^{2+} may be the regulating factor.

The dissociation of the dynein-microtubule complex is affected by Mg^{2+}-free ATP.

An increase in processivity would directly lead to an increase of dwell times of dynein molecules on microtubules by a decreased dissociation rate. We measured the influence of the ratio of Mg^{2+}-free ATP to Mg.ATP on the dissociation rate in stopped-flow experiments. A mixture of dynein and paclitaxel-stabilized microtubules was pre-incubated to form a stable complex in absence of ATP. Dissociation was then initiated by rapidly mixing the complex with Mg.ATP to a final concentration of 50 µM Mg.ATP. The dissociation of the microtubule-dynein complexes was detected by monitoring the light scattering. The observed data could be fitted best by a double exponential decay (**Fig. S1**) with a fast component R_D1 and a slow component R_D2. R_D1 represents the dissociation of the dynein-microtubule complex whereas R_D2 was reported to represent the slow de-polymerisation even of taxol-stabilized microtubules after dynein dissociation [38]. At a high ratio of Mg^{2+}-free ATP to Mg.ATP (hereafter called “high ratio”) we measured $R_D1_{\text{high ratio}}$ with 2.36 ± 0.34 s^{-1} (SEM, n=5) (**Fig. S1A**). Although a previously reported mixing artifact [38] partially concealed the initial ~150 ms of our stopped-flow experiments, $R_D1_{\text{low ratio}}$ at a low ratio of Mg^{2+}-free ATP to Mg.ATP (hereafter called “low ratio”) could be estimated to be at least 10 s^{-1} (n=5) (**Fig. S1B**). The >4-fold decrease in dissociation under high ratio conditions agrees well with the observed increase in processive stepping (**Fig. 1**).

Microtubule gliding activity of cytoplasmic dynein is affected by the ratio of Mg^{2+}-free ATP and Mg.ATP.

Our optical trap data suggests non-processive behaviour of dynein under low ratio conditions of Mg^{2+}-free ATP to Mg.ATP. At a constant low ratio of approximately 0.1, we achieved maximal gliding velocities at Mg.ATP concentrations of 0.1 mM and higher (**Fig. 2A**). To exclude limitations in ATP concentrations we, therefore, decided to perform gliding assays at constant saturating Mg.ATP concentrations of 0.1 mM. To determine possible differences in the motor velocity we carried out microtubule gliding assays with increasing ratios of Mg^{2+}-free ATP to Mg.ATP.

At constant 0.1 mM ATP and increasing concentrations of Mg^{2+} (0.1 to 20 mM) we observed decreasing microtubule gliding velocities from 0.47 µm/s at 0.1 mM Mg^{2+} to 0.22 µm/s at 20 mM Mg^{2+} (**Fig. 2B**, **Tab. S1**). Interestingly, this decrease in velocity occurred although the concentration of Mg.ATP increased from 0.038 to 0.099 mM. Yet, we calculated that at the same time the ratio of Mg^{2+}-free ATP to Mg.ATP decreased from 1.608 to 0.005 (**Tab. 1**), which indicates that the ratio of Mg^{2+}-free ATP to Mg.ATP and not the total Mg.ATP concentration determines the velocity. To confirm this effect of the ratio of Mg^{2+}-free ATP to Mg.ATP we varied the concentration of non-hydrolysable Mg^{2+}-free ATP from 7 to 400 µM while keeping the concentration of Mg.ATP constant at saturating 0.5 mM resulting in ratios of Mg^{2+}-free ATP to Mg.ATP of 0.014 and 0.801, respectively. With an increasing ratio the gliding velocity increased from 0.46 ± 0.02 µm/s to 0.71 ± 0.02 µm/s (**Fig. 2C, Tab. S2**).

The results from microtubule gliding assays and optical trap data were comparable. In both assays, we observed an increase of velocity with an increasing ratio of Mg^{2+}-free ATP to Mg.ATP.

Single molecule motility assays reveal increased productive binding and processive movement of dynein at high Mg^{2+}-free ATP.

The ability to characterize changes in processive behaviour in optical trap assays is limited by increasing load acting on the motor molecules upon movement. To measure single molecules in the absence of external load we performed single-molecule TIRF microscopy measurements [36]. We characterized the movement of individual dynein molecules tagged with a rhodamine-labelled intermediate-chain specific antibody [31] along immobilized microtubules under identical conditions as used in the gliding assays (**Fig.2C**; 7 µM or 400 µM Mg^{2+}-free ATP, at constant 500 µM Mg.ATP). Labelling of dynein with this antibody did not interfere with motility (**Fig. S4**).To emphasize possible effects we applied conditions favouring motor binding and processive stepping by lowering the ionic strength [39]. Processive movement was observed under both low and high ratio Mg^{2+}-free ATP to Mg.ATP conditions (**Fig. 3**) with run lengths of up to 5.5 µm in the latter case representing more than 680 consecutive 8 nm steps. However, the productive-binding frequency was 15-fold higher under high ratio conditions (0.092 runs*μm^{-1}*min^{-1}, total 687 µm microtubules analysed, **Tab. S2**) compared to low ratio conditions (0.006 runs*μm^{-1}*min^{-1}, total

2002 µm microtubules analyzed, **Tab. S2**). As the experimental spatial limit to discriminate stationary binding from movement was 3 pixels (~0.5 µm, see Methods) such reduced productive-binding frequency under low ratio conditions could reflect a lower dynein affinity for microtubules and/or shorter run lengths of dynein molecules. Therefore, a reduction of run lengths would also lead to a decreased apparent binding frequency. Under high ratio conditions individual dynein molecules moved significantly 1.5 times longer (median run length of 1.2 µm) than under low ratio conditions (median run length of 0.8 µm, Mann-Whitney test, $p < 0.01$, **Fig.3** and **Tab. S2**). Additionally, movement of individual dynein molecules under high ratio conditions was significantly 2-fold faster (0.93 µm s^{-1} compared to 0.47 µm s^{-1}, Mann-Whitney test, $p < 0.01$) than under low ratio conditions (**Fig.3** and **Tab. S2**). This observed difference in velocity under high and low ratio conditions is consistent with results gained from microtubule gliding experiments in the absence of the labelling antibody (**Fig. 2C**). The measured increase in run length of single dynein molecules under high ratio conditions is supported the optical trap experiments, again in the absence of dynein antibodies. Additional support for increased run lengths under high ratio conditions arises from the presented stopped-flow experiments, which showed decelerated detachment of dynein from microtubules compared to low ratio conditions. In the absence of ATP or dynein no directed motion along microtubules could be observed (**Fig. S2**).

The ATPase activity at high ratio conditions is increased

We performed ATPase assays and found a 2-fold increase in the calculated maximum microtubule-activated ATPase activity from 0.7 s^{-1} under low ratio to 1.4 s^{-1} under high ratio conditions and at microtubule concentrations of 1 µM or higher (**Fig. 4**, **Tab. S3**). The basal ATPase activity in the absence of MT was not changed.

Discussion

In single and multiple molecule experiments we found that the ratio of Mg^{2+}-free ATP to Mg.ATP influenced the motile behaviour of cytoplasmic dynein. At high ratio conditions (i.e., relatively high concentration of non-hydrolyzable Mg^{2+}-free ATP), dynein's velocity and run length, as well as its productive binding to microtubules and microtubule-activated ATPase activity were significantly higher than at low ratio conditions. To explain these results we propose a model dependent upon the nucleotide state of dynein's AAA4 domain (**Fig. 5**).

Binding of ATP at AAA4 keeps this module in a closed conformation as shown for yeast dynein bound to the non-hydrolysable ATP analogue AMPPNP [40] or human dynein in presence of ADP.Vi [8]. As Mg^{2+}-free ATP is not hydrolysable by dynein [24], binding of Mg^{2+}-free ATP, too, will arrest the binding site of AAA4 in this conformation that enables the linker to adopt a straight conformation and to dock on AAA5 [23,40]. A comparison of dynein's structures in the ADP.Vi and ADP state indicates a possible steric clash of the bent linker with AAA4 in the ADP-bound conformation during the power stroke [8]. This clash most likely prevents the formation of the linker's straight conformation. As several studies showed that AAA3 has to be in an ADP state for processive stepping [40-43] which requires an unhindered straightening of the linker, the described steric clash under ADP conditions must be caused by the nucleotide state of another AAA domain. Since AAA2 is enzymatically inactive the only remaining candidate is AAA4.

Based on the introduced reports on the nucleotide-dependent behaviour of dynein's AAA domains [8][23,24,40-43], in our proposed model AAA4 remains in the ATP state during fast, processive stepping. For AAA1 and AAA3 it has been shown that ATP hydrolysis is not synchronized between dynein's AAA+ domains [41] which likely holds true also for AAA4. The ATP state of AAA4 allows the bent linker to adopt a straight confirmation during the power stroke upon re-binding to the microtubule after P_i release form AAA1.

However, when the ATP in AAA4 is hydrolysed, the linker cannot adopt the straight conformation upon ATP hydrolysis in AAA1 due to a possible steric clash of the bent linker with the AAA2-AAA4 block [8]. Subsequently, the motor is locked in a weak microtubule binding state [44]. In the presence of load like in trap experiments, this leads to a detachment of the molecule from the microtubule resulting in the observed complete loss of processivity (**Fig. 1**). In the absence of load, the weakly bound motor can wait for a release of ADP from AAA4 and a subsequent binding of ATP to perform a power stroke. Consequently, this pathway requires more time, resulting in the observed ~2-fold decreased velocity in multi- (**Fig. 2**) and single-molecule (**Fig. 3**) assays, as well as the matching ~2-fold decreased ATPase rates (**Fig. 4**). Moreover, the prolonged weak binding state increases the detachment probability leading to the observed shorter run lengths (**Fig. 3**) and the increased dissociation rate (**Fig. S1**).

Our data, as well as this model, agree well with previously published data. In single molecule assays with yeast dynein processivity was increased ~2-fold when hydrolysis but not binding of Mg.ATP was abolished by a mutation of the Walker B motif of AAA4 [45], which is comparable to the binding of non-hydrolysable Mg^{2+}-free ATP. In contrast, mutations of the Walker A domain of AAA4 that inhibit nucleotide binding resulted in a decrease in dynein's velocity by ~70% [16], a highly decreased microtubule-activated ATPase activities [16], and a ~50% decrease in microtubule binding [46,47].

In vivo, either binding of non-hydrolysable Mg^{2+}-free ATP or a down-regulation of ATP hydrolysis in AAA4 would be the physiological equivalent of our experimental results. At physiological concentrations of magnesium and ATP in neurons [48] the cellular ratio of Mg^{2+}-free ATP to Mg.ATP is approximately 0.2. From our results (**Table 1**) we, therefore, assume that *in vivo* AAA4 might be preferentially in a processive Mg^{2+}-free ATP state. This assumption relies on different affinities of the different AAA+ domains to Mg.ATP and Mg^{2+}-free ATP, with AAA1 preferentially binding Mg.ATP and AAA4 containing Mg^{2+}-free ATP under physiological conditions.

More likely, hydrolysis in AAA4 is tightly regulated. Interestingly, in AAA4 domains of both yeast and *Dictyostelium* the catalytic glutamate is slightly tilted away from the nucleotide-binding pocket by a short helix directly after the Walker B motif indicating the need of a yet unknown conformational change before ATP hydrolysis [49]. This conformational change presumably acts as a switch between processive and non-processive stepping by retaining or cleaving ATP in AAA4, respectively. This switch could be linked to dynein’s C-terminal domain that has been shown to play an important role in the regulation of both processivity and maximal force [50]. Moreover, the switch could be triggered by binding to accessory proteins and complexes like dynactin [51,52], LIS1 [53], or the cargo adaptor BICD2 [54] that have been shown to increase cytoplasmic dynein’s processivity. As an example, point mutations in AAA4, but not in the Walker A or Walker B domains, of *Aspergillus nidulans* dynein have been shown to partially supress the phenotype of LIS1 loss [55] indicating a physiological role for regulation through AAA4. Additionally, dynein activity is impaired by a point mutation in the so-called pre-Sensor I region within AAA4, a potential secondary binding site for the linker domain, thus, leading to a combined phenotype of congenial motor neuron disease associated with focal areas of cortical malformation in humans [56]. Interestingly, the catalytic residues of AAA4 are poorly conserved in axonemal dynein, cytoplasmic dynein 2, and fungal cytoplasmic dynein [49]. This indicates that the ability to switch from processive to non-processive stepping might not be required for the physiological function of these motors.

Acknowledgements

We thank Petra Uta and Manuel Taft for help with protein purifications and for supplying technical instruments and assistance.

Figures legends

Fig. 1. Optical trap experiments. (A) Processive stepping of cytoplasmic dynein at 1 µM ATP and 0.1 mM $MgCl_2$. Please note the short life times of the early steps during the processive movement against the restoring trapping force. Initial steps are highlighted by a red line indicating the mean position of the position signal. Grid size 8nm. (B) Non-processive binding/release events of cytoplasmic dynein under low ratio conditions at 1 µM ATP and 1 mM $MgCl_2$. The histogram illustrates an approximately 8 nm apparent working stroke of dynein molecules towards the minus-end of the microtubule (shift of blue fit relative to positions of the free dumbbell shown in red).

Fig. 2. Microtubule gliding velocity of dynein at different concentrations of Mg.ATP, free Mg^{2+}, and Mg^{2+}-free ATP. (A) Gliding velocity at constant 1 mM $MgCl_2$ and increasing concentrations of Mg.ATP (0.001 to 0.5 mM). (B) Gliding velocity at constant 0.1 mM ATP and increasing concentration of Mg^{2+} (0.1, 5, 10 and 20 mM; n > 100 microtubules for every condition). (C) Gliding velocity at low (7 µM) and high (400 µM) concentration of Mg^{2+}-free ATP and constant concentration of Mg.ATP (0.5 mM). The average velocities were 0.46 µm/s (n = 30) and 0.71 µm/s (n = 34) for 7 µM and 400 µM Mg^{2+}-free ATP, respectively. Error bars show SEM. Data was distributed normally (D-Agostino-Pearson test), and the difference between both conditions was highly significant (t-test, $p < 0.001$).

Fig. 3. Processive movement of single native cytoplasmic dynein molecules. (A) Kymographs of dynein runs under high ratio (left panel) and low ratio conditions (right panel). The number of runs per µm microtubule per 60 seconds at a constant 500 µM Mg.ATP was more than 15-fold higher at 400 µM Mg^{2+}-free ATP (high ratio) (B) compared to 3 µM Mg^{2+}-free ATP (low ratio) (C). The median run lengths for high and low ratio conditions were 1.2 µm and 0.8 µm, respectively (B, C), and were significantly different (Mann-Whitney test, $p < 0.01$). (D, E) The respective median velocities were significantly higher for high ratio conditions (0.93 µm/s) compared to 0.47 µm/s for low ratio conditions (Mann-Whitney test, $p < 0.01$).

Fig. 4. The microtubule-activated ATPase rate of dynein increased at high ratio conditions while the basal ATPase rate remained unaffected. The dynein concentration was constant at 50 nM and the microtubule concentrations were 0, 0.2, 1, 5 and 10 µM tubulin dimer. The ATPase activities were then calculated to the ATPase s^{-1} per dynein molecule. Three experiments with three measurements each were averaged and are shown with SEM as error bars. Hyperbola fitting to the data revealed the K_m to be not affected. The maximal activated ATPase rates were 0.7 s^{-1} and 1.4 s^{-1} per dynein molecule for low and high ratio conditions, respectively.

Fig. 5. Proposed model for the molecular mechanism underlying the effect of the ratio of Mg^{2+}-free ATP to Mg.ATP on dynein's processive behaviour. The left-hand side resembles fast, processive stepping with AAA4 in the ATP state (solid arrows). Upon ATP hydrolysis in AAA4 dynein tends to slow down and/or prematurely detach from microtubules due to steric clashes of the linker with the AAA2-4 block. The inset on the right bottom illustrates the domain structure of dynein's AAA1-6 ring and the linker.

References

[1] Vallee, R.B., Williams, J.C., Varma, D. and Barnhart, L.E. (2004). Dynein: An ancient motor protein involved in multiple modes of transport. J Neurobiol 58, 189-200.

[2] Schroer, T.A. (2004). Dynactin. Annu Rev Cell Dev Biol 20, 759-79.

[3] McKenney, R.J., Huynh, W., Tanenbaum, M.E., Bhabha, G. and Vale, R.D. (2014). Activation of cytoplasmic dynein motility by dynactin-cargo adapter complexes. Science 345, 337-41 LID - 10.1126/science.1254198 [doi].

[4] Grotjahn, D.A., Chowdhury, S., Xu, Y., McKenney, R.J., Schroer, T.A. and Lander, G.C. (2018). Cryo-electron tomography reveals that dynactin recruits a team of dyneins for processive motility. Nat Struct Mol Biol 25, 203-207.

[5] Urnavicius, L., Lau, C.K., Elshenawy, M.M., Morales-Rios, E., Motz, C., Yildiz, A. and Carter, A.P. (2018). Cryo-EM shows how dynactin recruits two dyneins for faster movement. Nature 554, 202-206.

[6] Lee, I.G., Olenick, M.A., Boczkowska, M., Franzini-Armstrong, C., Holzbaur, E.L.F. and Dominguez, R. (2018). A conserved interaction of the dynein light intermediate chain with dynein-dynactin effectors necessary for processivity. Nat Commun 9, 986.

[7] Roberts, A.J., Kon, T., Knight, P.J., Sutoh, K. and Burgess, S.A. (2013). Functions and mechanics of dynein motor proteins. Nat Rev Mol Cell Biol 14, 713-26 LID - 10.1038/nrm3667 [doi].

[8] Schmidt, H. and Carter, A.P. (2016). Review: Structure and mechanism of the dynein motor ATPase. Biopolymers 105, 557-67 LID - 10.1002/bip.22856 [doi].

[9] Carter, A.P., Cho, C., Jin, L. and Vale, R.D. (2011). Crystal structure of the dynein motor domain. Science 331, 1159-65 LID - 10.1126/science.1202393 [doi].

[10] Kon, T., Oyama, T., Shimo-Kon, R., Imamula, K., Shima, T., Sutoh, K. and Kurisu, G. (2012). The 2.8 A crystal structure of the dynein motor domain. Nature 484, 345-50 LID - 10.1038/nature10955 [doi].

[11] Schmidt, H., Gleave, E.S. and Carter, A.P. (2012). Insights into dynein motor domain function from a 3.3-A crystal structure. Nat Struct Mol Biol 19, 492-7, S1 LID - 10.1038/nsmb.2272 [doi].

[12] Mocz, G. and Gibbons, I.R. (2001). Model for the motor component of dynein heavy chain based on homology to the AAA. Structure 9, 93-103.

[13] Kon, T., Sutoh, K. and Kurisu, G. (2011). X-ray structure of a functional full-length dynein motor domain. Nat Struct Mol Biol 18, 638-42 LID - 10.1038/nsmb.2074 [doi].

[14] Sakakibara, H. and Oiwa, K. (2011). Molecular organization and force-generating mechanism of dynein. FEBS J 278, 2964-79.

[15] Gibbons, I.R., Lee-Eiford, A., Mocz, G., Phillipson, C.A., Tang, W.J. and Gibbons, B.H. (1987). Photosensitized cleavage of dynein heavy chains. Cleavage at the "V1 site" by. J Biol Chem 262, 2780-6.

[16] Kon, T., Nishiura, M., Ohkura, R., Toyoshima, Y.Y. and Sutoh, K. (2004). Distinct functions of nucleotide-binding/hydrolysis sites in the four AAA modules. Biochemistry 43, 11266-74.

[17] Takahashi, Y., Edamatsu, M. and Toyoshima, Y.Y. (2004). Multiple ATP-hydrolyzing sites that potentially function in cytoplasmic dynein. Proc Natl Acad Sci U S A 101, 12865-9.

[18] Carter, A.P., Garbarino, J.E., Wilson-Kubalek, E.M., Shipley, W.E., Cho, C., Milligan, R.A., Vale, R.D. and Gibbons, I.R. (2008). Structure and functional role of dynein's microtubule-binding domain. Science 322, 1691-5 LID - 10.1126/science.1164424 [doi].

[19] Koonce, M.P. (1997). Identification of a microtubule-binding domain in a cytoplasmic dynein heavy. J Biol Chem 272, 19714-8.

[20] Kon, T., Imamula, K., Roberts, A.J., Ohkura, R., Knight, P.J., Gibbons, I.R., Burgess, S.A. and Sutoh, K. (2009). Helix sliding in the stalk coiled coil of dynein couples ATPase and microtubule. Nat Struct Mol Biol 16, 325-33 LID - 10.1038/nsmb.1555 [doi].

[21] Gibbons, I.R., Garbarino, J.E., Tan, C.E., Reck-Peterson, S.L., Vale, R.D. and Carter, A.P. (2005). The affinity of the dynein microtubule-binding domain is modulated by the. J Biol Chem 280, 23960-5.

[22] McNaughton, L., Tikhonenko, I., Banavali, N.K., LeMaster, D.M. and Koonce, M.P. (2010). A low affinity ground state conformation for the Dynein microtubule binding. J Biol Chem 285, 15994-6002 LID - 10.1074/jbc.M109.083535 [doi].

[23] Roberts, A.J., Malkova, B., Walker, M.L., Sakakibara, H., Numata, N., Kon, T., Ohkura, R., Edwards, T.A., Knight, P.J., Sutoh, K., Oiwa, K. and Burgess, S.A. (2012). ATP-driven remodeling of the linker domain in the dynein motor. Structure 20, 1670-80 LID - 10.1016/j.str.2012.07.003 [doi] LID - S0969-2126(12)00254-7 [pii].

[24] Shpetner, H.S., Paschal, B.M. and Vallee, R.B. (1988). Characterization of the microtubule-activated ATPase of brain cytoplasmic dynein. J Cell Biol 107, 1001-9.

[25] Walter, W.J., Koonce, M.P., Brenner, B. and Steffen, W. (2012). Two independent switches regulate cytoplasmic dynein's processivity and. Proc Natl Acad Sci U S A 109, 5289-93 LID - 10.1073/pnas.1116315109 [doi].

[26] Bingham, J.B., King, S.J. and Schroer, T.A. (1998). Purification of dynactin and dynein from brain tissue. Methods Enzymol 298, 171-84 FAU - Bingham, J B.

[27] Toba, S. and Toyoshima, Y.Y. (2004). Dissociation of double-headed cytoplasmic dynein into single-headed species and. Cell Motil Cytoskeleton 58, 281-9.

[28] Walter, W.J., Brenner, B. and Steffen, W. (2010). Cytoplasmic dynein is not a conventional processive motor. J Struct Biol 170, 266-9 LID - 10.1016/j.jsb.2009.11.011 [doi].

[29] Castoldi, M. and Popov, A.V. (2003). Purification of brain tubulin through two cycles of polymerization-depolymerization in a high-molarity buffer. Protein Expr Purif. 32, 83-8.

[30] Hyman, A., Drechsel, D., Kellogg, D., Salser, S., Sawin, K., Steffen, P., Wordeman, L. and Mitchison, T. (1991). Preparation of modified tubulins. Methods Enzymol 196, 478-85.

[31] Steffen, W., Hodgkinson, J.L. and Wiche, G. (1996). Immunogold localisation of the intermediate chain within the protein complex of cytoplasmic dynein. J Struct Biol 117, 227-35.

[32] Steffen, W., Lewalle, A. and Sleep, J. (2006) Chapter 4 - Optical Tweezers: Application to the Study of Motor Proteins A2 - Celis, Julio E. In Cell Biology (Third Edition) ed.^eds), pp. 37-45. Academic Press, Burlington.

[33] Schoenmakers, T.J., Visser, G.J., Flik, G. and Theuvenet, A.P. (1992). CHELATOR: an improved method for computing metal ion concentrations in. Biotechniques 12, 870-4, 876-9.

[34] Meijering, E., Dzyubachyk, O. and Smal, I. (2012). Methods for cell and particle tracking. Methods Enzymol 504, 183-200 LID - 10.1016/B978-0-12-391857-4.00009-4 [doi].

[35] Hinrichs, M.H., Jalal, A., Brenner, B., Mandelkow, E., Kumar, S. and Scholz, T. (2012). Tau protein diffuses along the microtubule lattice. J Biol Chem 287, 38559-68. doi: 10.1074/jbc.M112.369785.

[36] Pfeffer, T.J., Sasse, F., Schmidt, C.F., Lakamper, S., Kirschning, A. and Scholz, T. (2016). The natural diterpene tonantzitlolone A and its synthetic enantiomer inhibit cell proliferation and kinesin-5 function. Eur J Med Chem 112, 164-170.

[37] Webb, M.R. (1992). A continuous spectrophotometric assay for inorganic phosphate and for measuring. Proc Natl Acad Sci U S A 89, 4884-7.

[38] Porter, M.E. and Johnson, K.A. (1983). Transient state kinetic analysis of the ATP-induced dissociation of the dynein-microtubule complex. J Biol Chem 258, 6582-7.

[39] Vale, R.D., Funatsu, T., Pierce, D.W., Romberg, L., Harada, Y. and Yanagida, T. (1996). Direct observation of single kinesin molecules moving along microtubules. Nature 380, 451-3.

[40] Bhabha, G., Cheng, H.C., Zhang, N., Moeller, A., Liao, M., Speir, J.A., Cheng, Y. and Vale, R.D. (2014). Allosteric communication in the dynein motor domain. Cell 159, 857-68 LID - 10.1016/j.cell.2014.10.018 [doi] LID - S0092-8674(14)01306-3 [pii].

[41] Dewitt, M.A., Cypranowska, C.A., Cleary, F.B., Belyy, V. and Yildiz, A. (2015). The AAA3 domain of cytoplasmic dynein acts as a switch to facilitate microtubule. Nat Struct Mol Biol 22, 73-80 LID - 10.1038/nsmb.2930 [doi].

[42] Nicholas, M.P., Berger, F., Rao, L., Brenner, S., Cho, C. and Gennerich, A. (2015). Cytoplasmic dynein regulates its attachment to microtubules via nucleotide. Proc Natl Acad Sci U S A 112, 6371-6 LID - 10.1073/pnas.1417422112 [doi].

[43] Silvanovich, A., Li, M.G., Serr, M., Mische, S. and Hays, T.S. (2003). The third P-loop domain in cytoplasmic dynein heavy chain is essential for dynein. Mol Biol Cell 14, 1355-65.

[44] Miura, M., Matsubara, A., Kobayashi, T., Edamatsu, M. and Toyoshima, Y.Y. (2010). Nucleotide-dependent behavior of single molecules of cytoplasmic dynein on microtubules in vitro. FEBS Lett 584, 2351-5.

[45] Cho, C., Reck-Peterson, S.L. and Vale, R.D. (2008). Regulatory ATPase sites of cytoplasmic dynein affect processivity and force. J Biol Chem 283, 25839-45 LID - 10.1074/jbc.M802951200 [doi].

[46] Reck-Peterson, S.L. and Vale, R.D. (2004). Molecular dissection of the roles of nucleotide binding and hydrolysis in dynein's AAA domains in Saccharomyces cerevisiae. Proc Natl Acad Sci U S A 101, 14305.

[47] Reck-Peterson, S.L. and Vale, R.D. (2004). Molecular dissection of the roles of nucleotide binding and hydrolysis in dynein's AAA domains in Saccharomyces cerevisiae. Proc Natl Acad Sci U S A 101, 1491-5.

[48] Alvarez-Leefmans, F.J., Gamino, S.M. and Rink, T.J. (1984). Intracellular free magnesium in neurones of Helix aspersa measured with ion-selective micro-electrodes. J Physiol 354, 303-17.

[49] Carter, A.P. (2013). Crystal clear insights into how the dynein motor moves. J Cell Sci 126, 705-13 LID - 10.1242/jcs.120725 [doi].

[50] Nicholas, M.P., Hook, P., Brenner, S., Wynne, C.L., Vallee, R.B. and Gennerich, A. (2015). Control of cytoplasmic dynein force production and processivity by its C-terminal. Nat Commun 6, 6206 LID - 10.1038/ncomms7206 [doi].

[51] Kardon, J.R., Reck-Peterson, S.L. and Vale, R.D. (2009). Regulation of the processivity and intracellular localization of Saccharomyces. Proc Natl Acad Sci U S A 106, 5669-74 LID - 10.1073/pnas.0900976106 [doi].

[52] King, S.J. and Schroer, T.A. (2000). Dynactin increases the processivity of the cytoplasmic dynein motor. Nat Cell Biol 2, 20-4.

[53] Huang, J., Roberts, A.J., Leschziner, A.E. and Reck-Peterson, S.L. (2012). Lis1 acts as a "clutch" between the ATPase and microtubule-binding domains of the dynein motor. Cell 150, 975-86.

[54] Schlager, M.A., Hoang, H.T., Urnavicius, L., Bullock, S.L. and Carter, A.P. (2014). In vitro reconstitution of a highly processive recombinant human dynein complex. Embo J 33, 1855-68 LID - 10.15252/embj.201488792 [doi].

[55] Zhuang, L., Zhang, J. and Xiang, X. (2007). Point mutations in the stem region and the fourth AAA domain of cytoplasmic dynein heavy chain partially suppress the phenotype of NUDF/LIS1 loss in Aspergillus nidulans. Genetics 175, 1185-96.

[56] Fiorillo, C., Moro, F., Yi, J., Weil, S., Brisca, G., Astrea, G., Severino, M., Romano, A., Battini, R., Rossi, A., Minetti, C., Bruno, C., Santorelli, F.M. and Vallee, R. (2014). Novel dynein DYNC1H1 neck and motor domain mutations link distal spinal muscular atrophy and abnormal cortical development. Hum Mutat 35, 298-302.

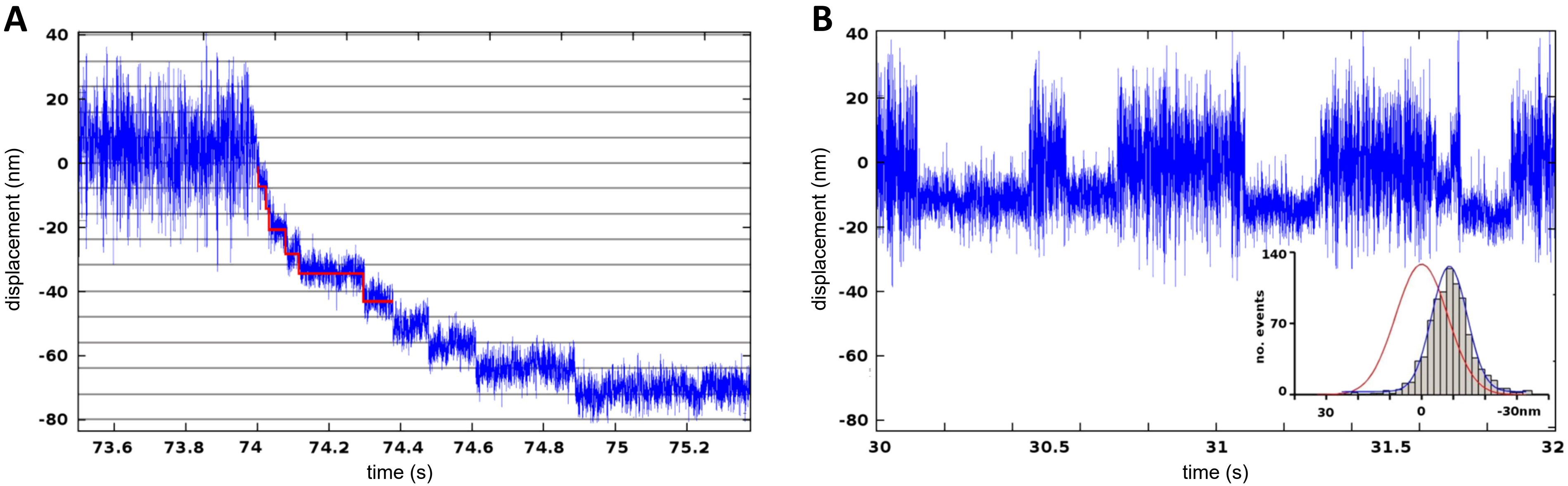
A
40
20
0
-20
-40
-60
-80
displacement (nm)
73.6
73.8
74
74.2
74.4
74.6
74.8
75
75.2
time (s)
B
40
20
0
-20
-40
-60
-80
displacement (nm)
30
30.5
31
31.5
32
time (s)
140
70
0
no. events
30
0
-30nm

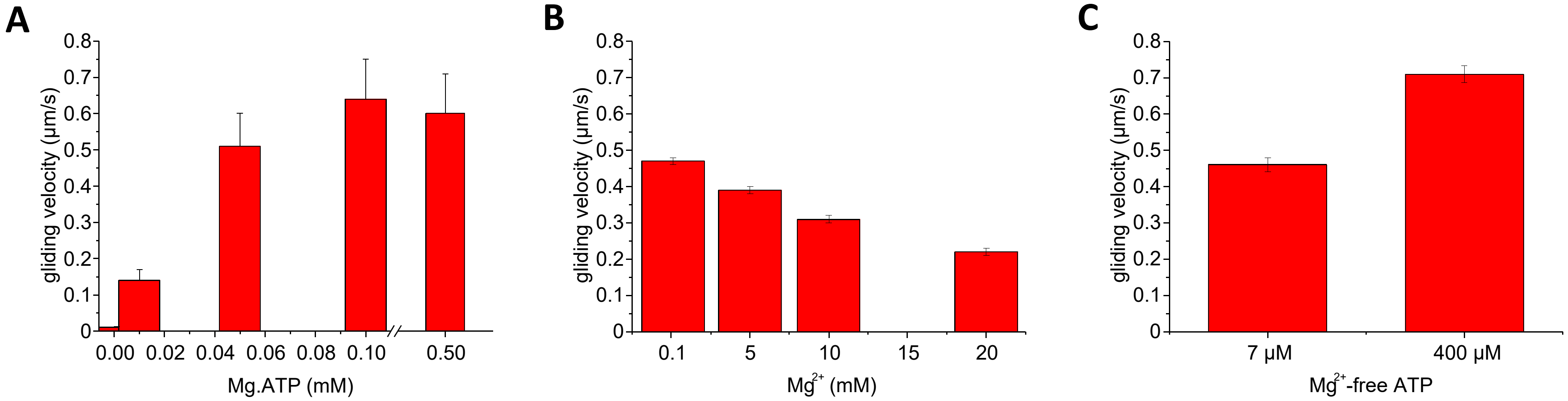
A
gliding velocity (µm/s)
0
0.1
0.2
0.3
0.4
0.5
0.6
0.7
0.8
0.00
0.02
0.04
0.06
0.08
0.10
0.50
Mg.ATP (mM)
B
gliding velocity (µm/s)
0
0.1
0.2
0.3
0.4
0.5
0.6
0.7
0.8
0.1
5
10
15
20
Mg2+ (mM)
C
gliding velocity (µm/s)
0
0.1
0.2
0.3
0.4
0.5
0.6
0.7
0.8
7 µM
400 µM
Mg2+-free ATP

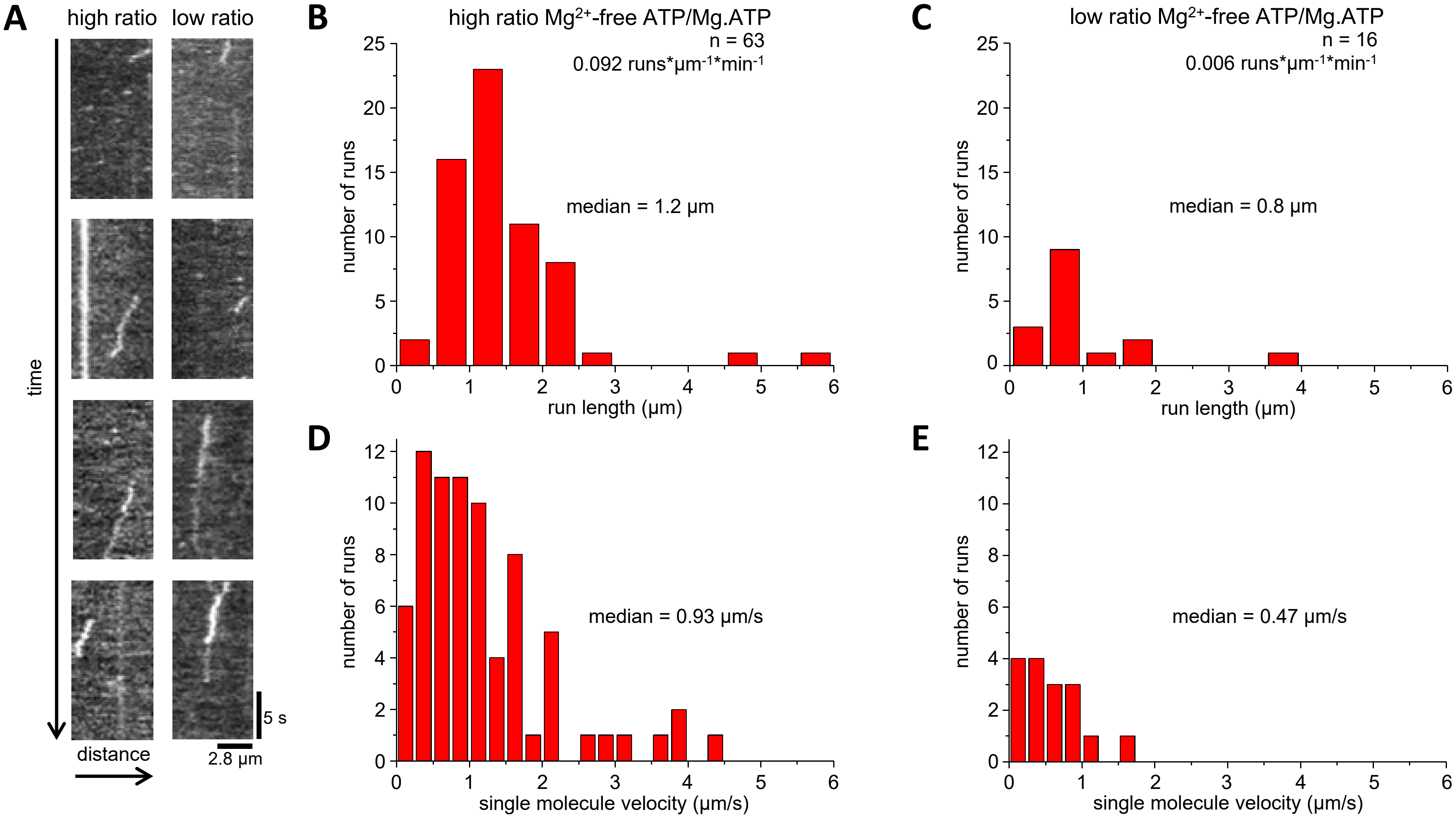
A
high ratio
low ratio
time
distance
5 s
2.8 μm
B
high ratio Mg2+-free ATP/Mg.ATP
n = 63
0.092 runs*μm-1*min-1
median = 1.2 μm
number of runs
run length (μm)
0 5 10 15 20 25
0 1 2 3 4 5 6
C
low ratio Mg2+-free ATP/Mg.ATP
n = 16
0.006 runs*μm-1*min-1
median = 0.8 μm
number of runs
run length (μm)
0 5 10 15 20 25
0 1 2 3 4 5 6
D
median = 0.93 μm/s
number of runs
single molecule velocity (μm/s)
0 2 4 6 8 10 12
0 1 2 3 4 5 6
E
median = 0.47 μm/s
number of runs
single molecule velocity (μm/s)
0 2 4 6 8 10 12
0 1 2 3 4 5 6

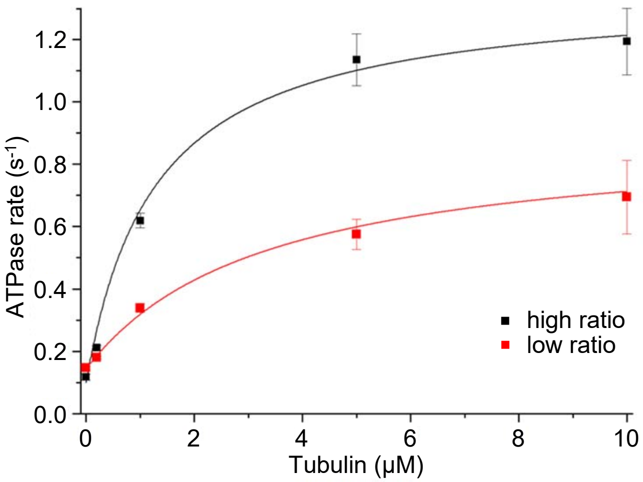
ATPase rate (s^{-1})
1.2
1.0
0.8
0.6
0.4
0.2
0.0
0
2
4
6
8
10
Tubulin (μM)
■ high ratio
■ low ratio

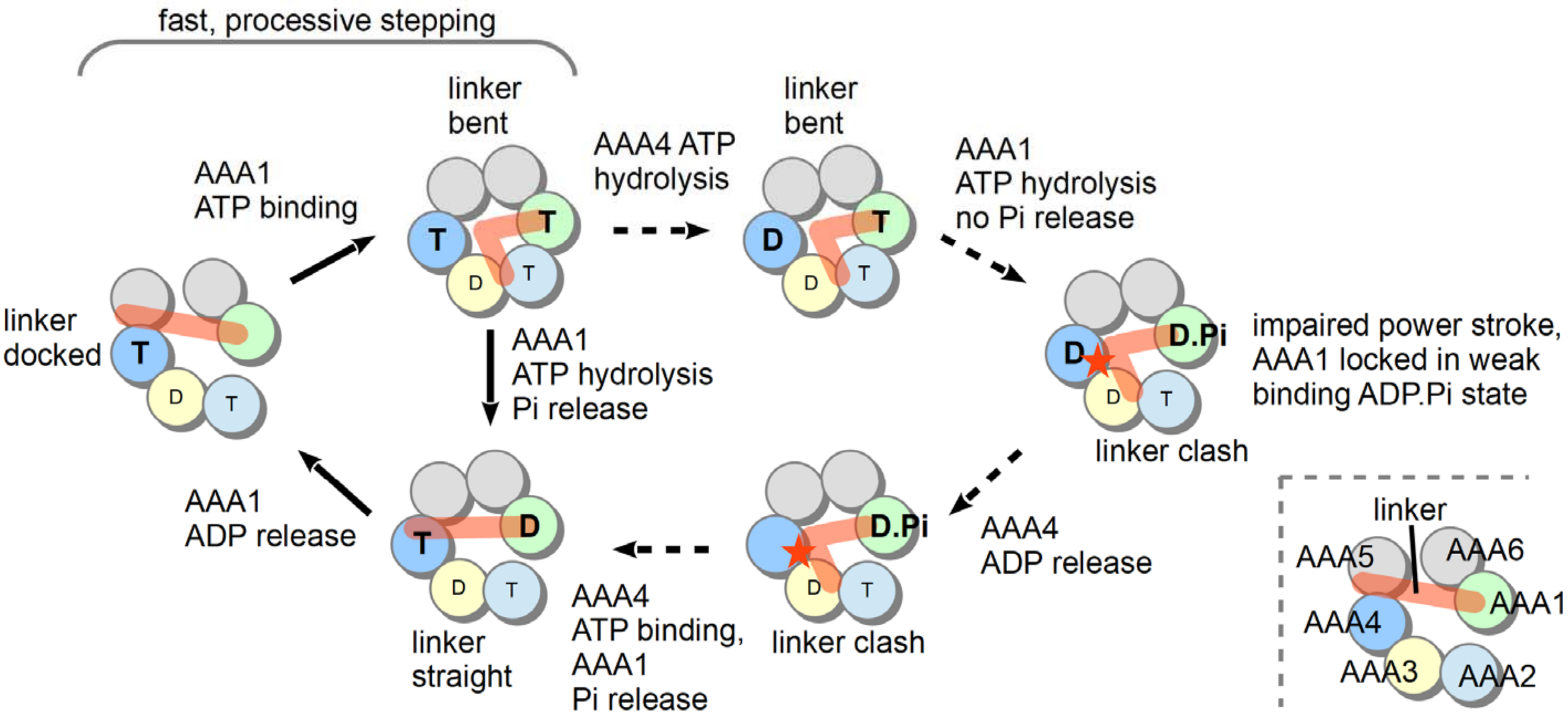fast, processive stepping
linker bent
linker bent
AAA1
ATP binding
AAA4 ATP
hydrolysis
AAA1
ATP hydrolysis
no Pi release
linker docked
T
D
T
T
T
D
T
D
T
D
T
AAA1
ATP hydrolysis
Pi release
D
D.Pi
D
T
impaired power stroke,
AAA1 locked in weak
binding ADP.Pi state
linker clash
AAA1
ADP release
T
D
D
T
D.Pi
D
T
AAA4
ADP release
linker
straight
AAA4
ATP binding,
AAA1
Pi release
linker clash
linker
AAA5
AAA6
AAA1
AAA4
AAA3
AAA2

Supporting information

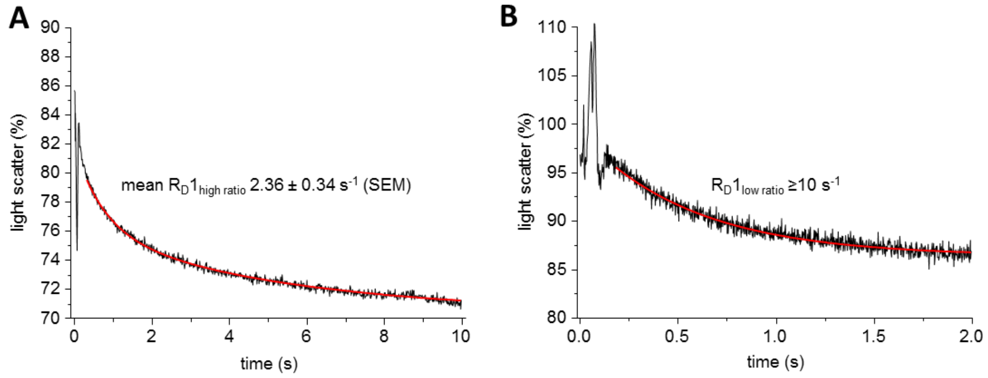

Fig. S1. Mg.ATP-induced dissociation of the dynein-microtubule complex is slowed down at high ratio conditions. Dissociation of the complex was induced by mixing the complex at high (A) and low (B) ratios of Mg^{2+}-free ATP to Mg.ATP (n=5 experiments each, red fits represent double exponential fits). The dissociation reactions revealed slower dissociation under high ratio conditions.

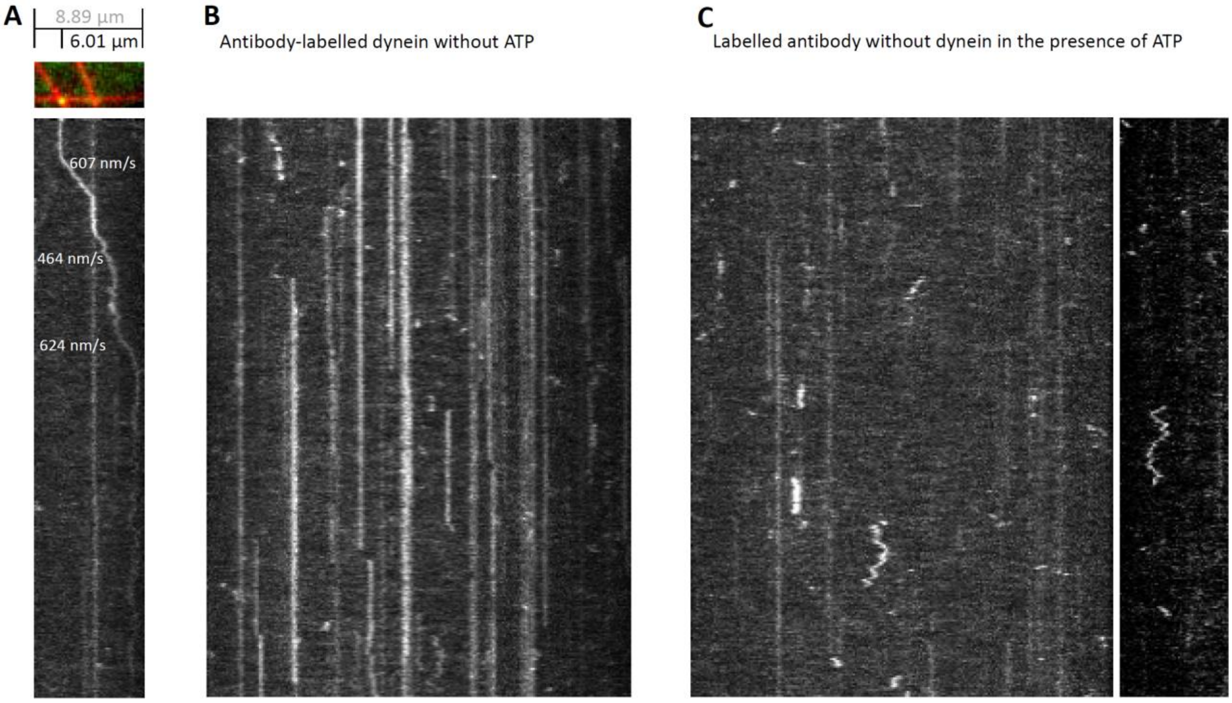
A
8.89 µm
6.01 µm
607 nm/s
464 nm/s
624 nm/s
B
Antibody-labelled dynein without ATP
C
Labelled antibody without dynein in the presence of ATP

Fig. S2. (A) Mg.ATP-driven motion of fluorescent antibody-labelled dynein along an immobilized microtubule under high ratio conditions (kymograph of 60 seconds). Note that pauses in dynein movement coincide with microtubule intersections. The given values describe the dynein velocities in the respective sections. Scale bars serve for figures A-C. (B) No motile dynein molecules were observed in the absence of Mg.ATP. (C) Dynein-free rhodamine-labelled dynein intermediate-chain specific antibodies [1] showed reduced binding and no directed motion along microtubules. As reported before [2] undirected, diffusive movement was observed.

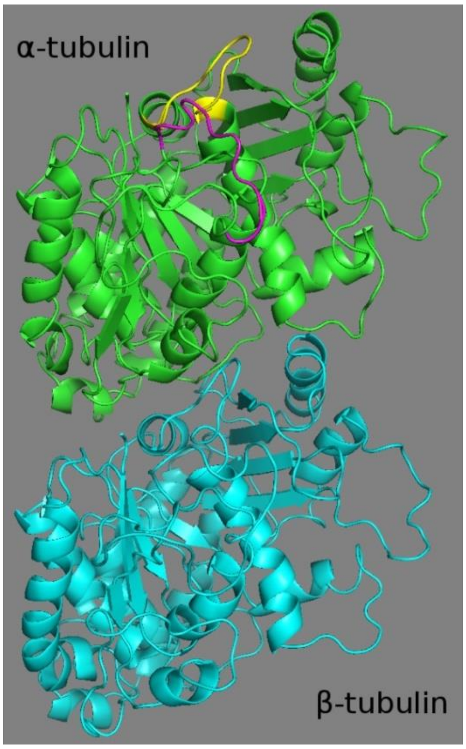

Fig. S3. Polyclonal antibodies specific for the minus-end of microtubules were raised in rabbits against two synthetic peptides from bovine α-tubulin. As highlighted in yellow and magenta (based on PDB structure 1JFF) the following peptides of α-tubulin have been used for antibody production: peptide 1: aa31-40 (QPDGQ MPSDK) and peptide 2: aa242-255 (LRFDG ALNVD LTEF).

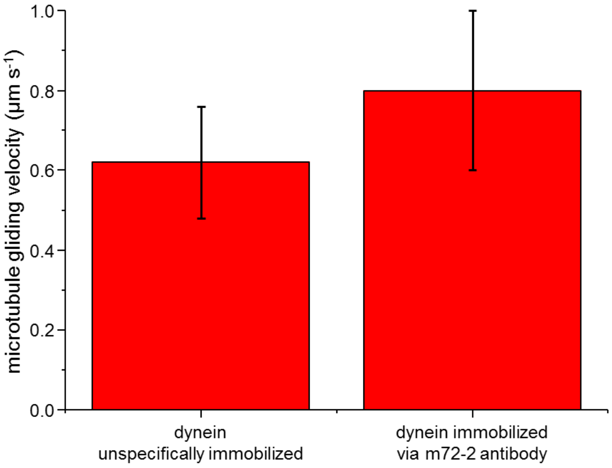

Fig. S4. Microtubule gliding velocity on dynein molecules attached unspecifically or via dynein-binding m74-2 antibodies to the surface of a flow chamber. Binding of the m74-2 antibody to the IC of dynein molecules did not interfere with motor function. The presence of the antibody had just a small effect on dynein motility and led to slightly faster microtubule gliding (0.8 µm/s ± 0.2 µm/s; SD, right) compared to 0.62 µm/s (± 0.14 µm/s; SD) in control experiments (left).

Table S1. The *in vitro* microtubule gliding velocity went down with increasing concentrations of Mg^{2+} (Fig. 2B). Assays were performed at a constant concentration of 0.1 mM ATP with increasing concentrations of Mg^{2+} (0.1, 5, 10 and 20 mM). The gliding velocities of fluorescently labelled microtubules were measured and the given errors are the SEM of measured values (n>100 for each condition).

$MgCl_2$ (mM)	0.1	5	10	20
Velocity (µm/s)	0.47 +/- 0.01	0.39 +/- 0.01	0.31 +/- 0.01	0.22 +/- 0.01

Table S2. Summary of functional measurements at low and high ratio conditions. The gliding velocities (data from Fig. 2; errors represent SEM) were significantly different ($p < 0.001$). In SMM data (from Fig. 3) both, the velocity and the run length were significantly different for low and high ratio conditions ($p < 0.01$ and $p < 0.05$, respectively).

Experiment	**Measured Value**	**Low Ratio** 7 µM Mg^{2+}-free ATP	**High Ratio** 400 µM Mg^{2+}-free ATP
Gliding Assay	Velocity (µm/s)	0.46 +/-0.019	0.71 +/- 0.023
SMM Assay	Number of runs	16	63
	Analyzed MT length (µm)	2002	687
	Runs/µm/min	0.006	0.092
	Velocity (µm/s) (median)	0.47	0.93
	Run Length (µm) (median)	0.8	1.2

Table S3. Dynein ATPase Assay. A 2-fold increase in the activated ATPase activity agreed with the different velocities in the SMM assay (Fig. 3). The activated ATPase was measured at the same conditions as the gliding assay (Fig. 2B and Table S2) at a dynein concentration of 0.07 mg/ml and with several concentrations of microtubules. The measured ATPase activities were calculated to the ATPase s^{-1} per dynein. The errors are the SEM from three different experiments with three replicates each. The K_m was not affected by Mg^{2+}-free ATP. The microtubule-activated ATPase was higher at high ratio conditions for microtubule concentrations between 1 to 10 µM tubulin. The calculated maximum activated ATPase activity was 0.7 and 1.4 s^{-1} for low and high ratio conditions, respectively.

	Low Ratio	**High Ratio**
K_m (µM)	1.0 +/- 0.6	1.1 +/- 0.3
Microtubule (µM)	**ATPase rate in s^{-1}**	
0	0.15 +/- 0.01	0.12 +/- 0.01
0.2	0.18 +/- 0.01	0.21 +/- 0.01
1	0.34 +/- 0.01	0.62 +/- 0.02
5	0.57 +/- 0.05	1.14 +/- 0.08
10	0.69 +/- 0.12	1.19 +/- 0.11
Max. activated ATPase rate in s^{-1} (calculated)	0.7 +/- 0.1	1.4 +/- 0.1

References

[1] Steffen, W., Hodgkinson, J.L. and Wiche, G. (1996). Immunogold localisation of the intermediate chain within the protein complex of cytoplasmic dynein. J Struct Biol 117, 227-35.

[2] Hinrichs, M.H., Jalal, A., Brenner, B., Mandelkow, E., Kumar, S. and Scholz, T. (2012). Tau protein diffuses along the microtubule lattice. J Biol Chem 287, 38559-68. doi: 10.1074/jbc.M112.369785.